

Frontogenesis of the Angola-Benguela Frontal Zone

Shunya Koseki¹, Hervé Giordani², and Katerina Goubanova^{3,4},

1. Geophysical Institute, University of Bergen, Bergen/Bjerknes Centre for Climate Research, Norway
2. Centre National de Recherches Météorologiques, MÉTÉO-France, Toulouse, France
3. Centro de Estudios Avanzados en Zonas Áridas, La Serena, Chile
4. CECI/CERFACS-CNRS, Toulouse, France

Correspondence to Shunya Koseki

Email: Shunya.Koseki@gfi.uib.no

Address: Geophysical Institute, University of Bergen, Postboks 7803, 5020, Bergen, Norway

1 **Abstract**

2 A diagnostic analysis of the climatological annual mean and seasonal cycle of the
3 Angola Benguela Frontal Zone (ABFZ) is performed applying an ocean frontogenesis
4 function (OFGF) to the ocean mixing layer (OML). The OFGF reveals that the
5 meridional confluence and vertical tilting terms are the most dominant contributors to
6 the frontogenesis of the ABFZ. The ABFZ shows a well-pronounced semi-annual
7 cycle with two maximum (minimum) peaks in April-May and November-December
8 (February-March and July-August). The development of the two maxima of
9 frontogenesis is due to two different physical processes: enhanced tilting from March
10 to April and meridional confluence from September to October. The strong meridional
11 confluence in September-October is closely related to the seasonal southward
12 intrusion of tropical warm water to the ABFZ that seems to be associated with the
13 development of the Angola Dome northwestern of the ABFZ. The strong tilting effect
14 from March to April is attributed to the meridional gradient of vertical velocities
15 whose effect is amplified in this period due to increasing stratification and shallow
16 OML depth. The proposed OFGF can be viewed as a tool to diagnose the performance
17 of Coupled General Circulation Models (CGCMs) that generally fail in simulating
18 realistically the position of the ABFZ, which leads to huge warm biases in the
19 southeastern Atlantic.

20

21

22

23

25 1. Introduction

26 The Angola-Benguela Frontal Zone (ABFZ, see Fig. 1), situated off the coast
27 of Angola/Namibia, is a key oceanic feature in the southeastern Atlantic Ocean. The
28 ABFZ separates the warm sea water of the Angola Current (e.g., Kopte et al., 2017)
29 from the cold sea water associated with the Benguela Current/upwelling system (e.g.,
30 Mohrholz et al., 2004; Colberg and Reason, 2006; Veitch et al., 2006; Colberg and
31 Reason, 2007; Fennel et al., 2012; Goubanova et al., 2013; Junker et al., 2015; Junker
32 et al., 2017; Vizy et al., 2018). The ABFZ is characterized by smaller spatial extent
33 and weaker SST gradient compared to the major oceanic fronts generated by the
34 western boundary currents (Fig. 1). However, due to its near coastal location, the
35 ABFZ plays important roles for the southern African continent, strongly impacting
36 local marine ecosystem (e.g., Auel and Verheye, 2007; Chavez and Messié, 2009) and
37 regional climate (Hirst and Hastenrath, 1983; Rouault et al. 2003; Hansingo and
38 Reason, 2009; Manhique et al., 2015). In particular, the main mode of interannual
39 variability of SST in the ABFZ, so-called Benguela Niño/Niña (e.g., Florenchie et al.,
40 2003; Rouault et al., 2017), influences the local rainfall along the southwestern
41 African coast of Angola and Namibia via moisture flux anomalies associated with the
42 SST anomalies (Rouault et al., 2003; Lutz et al., 2015) and tends to have a remote
43 impact on rainfall activity over the southeastern African continent (e.g., Manhique et
44 al., 2015).

45 The ABFZ region also poses one of the major challenges for the global climate
46 modeling community. Most CGCMs exhibit a huge warm SST bias in the ABFZ (e.g.,
47 Zuidema et al., 2016) and fail to reproduce the realistic SST, its seasonal cycle and the

right location of the ABFZ (e.g., Koseki et al., 2017). While Colberg and Reason (2006) and Giordani et al. (2011) concluded that the position of the ABFZ is controlled to a large extent by the local wind stress curl, Koseki et al. (2018) elucidated that the local wind stress curl bias in CGCMs contributes partly to the warm SST bias in the ABFZ via erroneous intrusion of tropical warm water, which is induced by a negative wind stress curl and enhanced Angola Current. In order to understand comprehensively the sources of such model biases, one need to understand the processes of generation of the ABFZ.

Previous studies have focused mainly on the SST variability at interannual to decadal scales in the ABFZ, and/or on its impacts on regional climate are well-studied (e.g., Rouault et al., 2003; Lutz et al., 2015; Vizy et al., 2018). Whereas Morholz et al. (1999) analyzed the ABFZ during a particular event in 1999, to our knowledge, there are few or no works quantitatively investigating dynamical and thermodynamical processes responsible for climatological state of the ABFZ and its seasonal cycle. A dynamical diagnosis for the SST front in the north of the Atlantic Cold Tongue (e.g., Hasternrath and Lamb, 1978; Giordani et al., 2013) was proposed by Giordani and Caniaux (2014, hereafter referred as GC2014). The frontogenetic function they use is, in general, adapted to explore sources of frontogenesis of atmospheric synoptic-scale cyclones in the extratropics (e. g., Keyser et al., 1988; Giordani and Caniaux, 2001). Using a frontogenetic function GC2014 showed clearly that the convergence associated with the northern South Equatorial Current and Guinea Current forces the SST-front intensity (frontogenetic effect) whereas mixed-layer turbulent flux destroys the SST-front (frontolytic effect). Fundamentally, the frontogenetic function consists of three mechanical terms (confluence, shear and tilting) and two thermodynamical terms (adiabatic heating and vertical mixing). Around the ABFZ, all these terms can be

considered as contributors to the frontogenesis due to: (1) the confluence zone associated with the southward Angola and northward Benguela currents (confluence and shear). (2) strong coastal upwelling (tilting) associated with Benguela current; (3) spatial variations in radiative fluxes induced by stratocumulus cloud deck (diabatic heating related to radiation) associated with the cold SST and subsidence due to St. Helena Anticyclone (e.g., Klein and Hartmann, 1993; Pfeifroth et al., 2012). So far, the relative roles of these different processes in the frontogenesis of the ABFZ still need to be investigated.

In this study, following the fundamental philosophy of GC2014, we attempt to understand the mechanisms responsible for the climatological ABFZ development at seasonal scale based on a first-order estimation. We propose an ocean frontogenetic function in a different way from GC2014 focusing on the ocean-mixed layer mean front. The structure of the remainder of this paper is as follows: Section 2 gives details of data set used in this study. In section 3, we derive the ocean frontogenetic function. Section 4 provides a description of the climatological state around the ABFZ. In section 5, we apply our diagnostic methodology to the ABFZ and determine the main terms of the frontogenetic function controlling its annual mean and seasonal cycle. The associated processes are discussed in section 6. Finally we summarize and make some concluding remarks in section 7.

2. Data

For an overview of SST and its meridional gradient in the ABFZ and evaluation of the reanalysis data, we employ the Optimum Interpolated Sea Surface Temperature (OISST, Reynolds et al., 2002) released by National Oceanic and

Atmospheric Administration (NOAA) that has a quarter degree of horizontal resolution and daily temporal resolution from 1982 to 2010. For the 3-dimensional diagnostic analysis of the ABFZ, we utilize 1-hour forecast data of Climate Forecast System Reanalysis (CFSR, Saha et al., 2010) developed by the National Centers for Environmental Prediction (NCEP). The ocean component of this system is based on MOM version 4p0d (Griffies et al., 2004) and implements data assimilation for the forecast. This system provides 6-hourly data with a 0.5 degree horizontal resolution and 70 vertical layers for ocean. This resolution is relatively coarse compared to the resolution of simulations performed with regional ocean models in a forced mode using wind forcing from satellite products. However, the advantage of a coupled ocean-atmosphere system CFSR is that it allows avoiding spurious effects in wind forcing over coastal regions resulting from the extrapolation in a 25-50km width coastal fringe where the wind cannot be observed by scattermeters (Astudillo et al., 2017). Moreover, the wind satellite products are generally available for only a relatively short time period, limiting investigation of long-term climatology and seasonal cycle. In this paper we will analyze daily-means (the procedure of data post-processing is given in Supplemental Information) and utilize the CFSR outputs of velocity (horizontal and vertical), potential temperature, net surface heat flux, ocean mixing layer depth, and sea surface height.

3. Ocean Frontogenesis Function

The ocean frontogenetic function (OFGF) is defined and applied to the ocean mixing layer (OML) in order to propose a dynamical diagnosis of the maintenance/generating process of the ABFZ. Following GC2014, we use the OFGF

as a tool to unravel the Lagrangian (pure) sources of the oceanic front. While there is plentiful literature investigating the ocean front dynamics (e.g., Dinniman and Rienecker, 1999), the concept of this OFGF has been hardly referred to. The Lagrangian frontogenesis function, F , is defined as

$$F \equiv \frac{d}{dt} \left(\frac{\partial \theta}{\partial y} \right) \quad (3.1),$$

where θ is the temperature. While the frontogenetic function is generally defined as the square of the horizontal gradient of the temperature (e.g., GC2014), our study employs only the meridional gradient of the temperature because the ABFZ SST-gradient is oriented South-North. The right hand side of Eq. 3.1 can be written as,

$$\begin{aligned} \frac{d}{dt} \left(\frac{\partial \theta}{\partial y} \right) &= u \frac{\partial}{\partial x} \left(\frac{\partial \theta}{\partial y} \right) + v \frac{\partial}{\partial y} \left(\frac{\partial \theta}{\partial y} \right) + w \frac{\partial}{\partial z} \left(\frac{\partial \theta}{\partial y} \right) + \frac{\partial}{\partial t} \left(\frac{\partial \theta}{\partial y} \right) \\ &= -\frac{\partial u}{\partial y} \frac{\partial \theta}{\partial x} - \frac{\partial v}{\partial y} \frac{\partial \theta}{\partial y} - \frac{\partial w}{\partial y} \frac{\partial \theta}{\partial z} + \frac{\partial}{\partial y} \left(\frac{\partial \theta}{\partial t} + u \frac{\partial \theta}{\partial x} + v \frac{\partial \theta}{\partial y} + w \frac{\partial \theta}{\partial z} \right) \\ &= -\frac{\partial u}{\partial y} \frac{\partial \theta}{\partial x} - \frac{\partial v}{\partial y} \frac{\partial \theta}{\partial y} - \frac{\partial w}{\partial y} \frac{\partial \theta}{\partial z} + \frac{\partial}{\partial y} \left(\frac{d\theta}{dt} \right) \end{aligned}$$

and using
$$\frac{d\theta}{dt} = -\frac{\partial \overline{w'\theta'}}{\partial z}$$

we obtain

$$\frac{d}{dt} \left(\frac{\partial \theta}{\partial y} \right) = -\frac{\partial u}{\partial y} \frac{\partial \theta}{\partial x} - \frac{\partial v}{\partial y} \frac{\partial \theta}{\partial y} - \frac{\partial w}{\partial y} \frac{\partial \theta}{\partial z} + \frac{\partial}{\partial y} \left(-\frac{\partial \overline{w'\theta'}}{\partial z} \right) \quad (3.2)$$

Here, u , v , and w denote the zonal, meridional, and vertical current velocity, respectively. Equation 3.2 describes the processes that act to generate/destroy the ocean front. The terms $-\frac{\partial u}{\partial y} \frac{\partial \theta}{\partial x}$, $-\frac{\partial v}{\partial y} \frac{\partial \theta}{\partial y}$, and $-\frac{\partial w}{\partial y} \frac{\partial \theta}{\partial z}$ are the contributions due to the mechanical processes: shear, convergence and tilting, respectively. The shear term

represents conversion of the zonal temperature gradient into meridional gradient by zonal current shear. In particular, the cool SST associated with the Benguela upwelling creates a strong zonal gradient in the south of the ABFZ (e.g., Morholz et al., 1999). The shear term can explain the conversion of such zonal gradient into meridional gradient. The convergence term represents strengthening/weakening of the meridional temperature gradient by convergence/divergence of meridional current. The tilting term represents conversion of the vertical stratification into meridional gradient by meridional shear of vertical velocity.

The fourth term is a thermodynamical term due to exchange of heat associated with the turbulent heat flux (surface heat flux is included into $w'\theta'$, it is the surface boundary condition). The contribution due to the second order horizontal diffusion is ignored for simplicity.

Since within the OML the temperature is fairly uniform (cf. Fig. 2 to compare the SST and OML-averaged temperature), we consider the OFGF with the mixed-layer mean quantities. With the approximation that temperature is independent of the depth in the OML (e.g., Kazmin and Rienecker, 1996; Tozuka and Cronin, 2014), Eq. 3.2 can be expressed as,

$$\frac{d}{dt} \left(\frac{\partial \theta_{oml}}{\partial y} \right) = - \frac{\partial u_{oml}}{\partial y} \frac{\partial \theta_{oml}}{\partial x} - \frac{\partial v_{oml}}{\partial y} \frac{\partial \theta_{oml}}{\partial y} - \frac{\partial (w_b + w_e)}{\partial y} \frac{\Delta \theta}{D} + \frac{\partial}{\partial y} \left(\frac{Q_s + Q_b}{\rho C_p D} \right) \quad (3.3),$$

where, the subscript of *oml* indicates the OML-mean quantity estimated by,

$$A_{oml} = \frac{1}{D} \int_D^{surface} A \cdot dz$$

where D denotes the OML depth, that is, the terms with subscript *oml* include the changes in the OML implicitly. Although the horizontal velocity is a function of depth even in the OML, the horizontal mechanical terms in Eq. 3.3 can be written in terms of OML-mean quantities because **the production is linear in u and v as long** as the temperature is independent of depth in the OML. w_b , w_e , $\Delta\theta$ and D represent the vertical velocity, the entrainment velocity, the temperature jump at the bottom of the OML, and the OML depth, respectively. According to Moissan and Niller (1998), the entrainment velocity at the bottom of the OML is estimated by

$$w_e = \frac{\partial D}{\partial t} + \mathbf{u}_b \cdot \nabla D$$

here, \mathbf{u}_b is the horizontal velocity at the bottom of the OML. $\Delta\theta$ is estimated as the difference between the OML-mean temperature and the **temperature just below the OML**. We use constant values for sea water density, ρ (1000 kg/m³) and isobaric specific heat of sea water, C_p (4200 Jkg⁻¹K⁻¹). The vertical mixing term is replaced with Q_s and Q_b , where $Q_s = (-\overline{w'\theta'})_{z=0}$ is the surface net heat flux at the top of OML (downward is positive in this study) and $Q_b = (-\overline{w'\theta'})_{z=D}$ represents the vertical mixing at the bottom of the OML, *i.e.*, in the thermocline. We assume that there is no penetration of shortwave radiation beyond the OML to deeper ocean layers. Because the vertical turbulent mixing term at the mixed-layer base Q_b is represented according to K-profile parameterization in OAGCMs; it will be not addressed explicitly in this study as it is not possible to estimate it from the reanalysis outputs.

While Eq. 3.3 is Lagrangian form of the OFGF, the equation can be also expressed in Eulerian form as below:

$$\begin{aligned}
182 \quad \frac{\partial}{\partial t} \left(\frac{\partial \theta_{oml}}{\partial y} \right) = & \underbrace{-\frac{\partial u_{oml}}{\partial y} \frac{\partial \theta_{oml}}{\partial x}}_{\text{SHER}} - \underbrace{\frac{\partial v_{oml}}{\partial y} \frac{\partial \theta_{oml}}{\partial y}}_{\text{CONF}} - \underbrace{\frac{\partial w_b}{\partial y} \frac{\Delta \theta}{D}}_{\text{TILT}} + \underbrace{\frac{\partial}{\partial y} \left(\frac{Q_s}{\rho C_p D} \right)}_{\text{SFLX}} + \underbrace{\text{residual}}_{\text{RESD}} \quad (3.4).
\end{aligned}$$

183 In this equation, the kinematic $\left(-\frac{\partial w_e}{\partial y} \frac{\Delta \theta}{D} \right)$ and diabatic Q_b entrainment terms and, the
184 horizontal and vertical advection terms of $\partial \theta_{oml} / \partial y$ are included in RESD. Accurate
185 estimation of the entrainment terms are not possible from CFSR outputs and the
186 horizontal and vertical advection effects are not related to Lagrangian sources of the
187 frontogenesis. In the remainder of this paper, the shear term will be referred to as
188 SHER, the confluence as CONF, the tilting as TILT, the thermodynamic term as
189 SFLX and the residual as RESD.

190 Note that basically, our climatology is a 29-year mean from 1982 to 2010
191 (procedure of making daily climatology of temperature meridional gradient and
192 OFGF are described in supplemental information). However, some years do not have
193 OML data at some grid points around the coastal region. For these grid points, we
194 make the climatology only for available years. For example, the smallest number in
195 the focusing ABFZ is 16 years at 16.25 °S.

196

197 4. Overview of the ABFZ and its Seasonal Cycle in CFSR data

198 Before the dynamical diagnosis is performed, we provide a brief overview of
199 the main feature of the ABFZ. The maximum of the ABFZ (up to 1.4 °C/100km) is
200 located at 16 °S just near the coast (Fig.1b). Figure 2a shows a seasonal cycle of the
201 temperature and its meridional gradient obtained from the satellite product OISST. In
202 this study, the maximum value of the meridional SST gradient is defined as the
203 intensity of the ABFZ. The core (SST meridional gradient exceeds 1.0 °C/100km) of

the ABFZ always lies between 17 °S and 15 °S. At climatological seasonal scale, the location of the ABFZ exhibits rather weak variability compared to strong interannual variability associated with the Benguela Niños that push the ABFZ southward due to the southward intrusion of tropical warm water (e.g., Gammelsrød et al. 1998; Veitch et al., 2006; Rouault et al., 2017). For instance, Rouault et al. (2017) showed that during Benguela Niño 2010-2011 the ABFZ displaced southward as far as 20°S. The intensity of the ABFZ shows a pronounced seasonal cycle: there are two peaks of the strength in April-May and November-to-December, respectively. The semi-annual cycle of the ABFZ will be examined in more details in the following sections. Figures 2b and c evidence that the CFSR reanalysis reproduces realistically the annual cycle of the ABFZ, and that the annual cycle of the corresponding OML-mean temperature meridional gradient is representative of the annual cycle of the SST meridional gradient in terms of both timing and intensity of the two annual peaks. This latter result justifies our approach to diagnose the frontogenesis of the ABFZ with the OML-mean quantities.

5. Diagnosis on the frontogenesis of the ABFZ

In this section, we investigate the frontogenesis of the ABFZ diagnostically applying the OFGF described in Section 3. Figure 3 illustrates the climatological annual-mean oceanic dynamical fields. The southwestward Angola and northwestward Benguela alongshore currents collide just south of the ABFZ. Seaward from the ABFZ, a strong westward current is detected. An intense upwelling (vertical velocity at the bottom of OML exceeding 0.18 m/day) is generated along the coast in the Benguela Current region. A local maximum of upwelling in the ABFZ

(approximately 17 °S) corresponds to one of the most vigorous upwelling cells in the region, namely Kunene upwelling cell (Kay et al., 2018). Note also a relatively weak downwelling cell (vertical velocity down to -0.06 m/day) just seaward from the Kunene upwelling cell.

5.1 Annual-mean state

Figure 4 presents the annual-mean climatology of the 5 forcing/source terms of the OFGF superimposing the meridional gradient of the OML-mean temperature. SHER works frontolytically (destroying the front, about $-2\text{ }^{\circ}\text{C}/100\text{ km}\times 10^{-7}\text{ s}^{-1}$) in the most parts of the ABFZ except just near the coast at 17 °S, although its frontogenetic (generating front) contribution here is rather weak here (less than $2\text{ }^{\circ}\text{C}/100\text{ km}\times 10^{-7}\text{ s}^{-1}$). CONF has on average an intense frontogenetic contribution to the ABFZ (up to $5\text{ }^{\circ}\text{C}/100\text{ km}\times 10^{-7}\text{ s}^{-1}$), especially offshore around 16 °S, the latitude where the ABFZ is centered (Fig. 2). The frontogenetic effect of CONF is consistent with GC2014 (the frontogenesis of the SST front associated with the equatorial Atlantic cold tongue is due to the confluence of northern South Equatorial Current and Guinea Current) and can be expected because the warm and cold currents meet around the ABFZ. Note however a small zone just near the coast at 16 °S where the CONF is frontolytic. This local frontolytic contribution is overcompensated by a strong frontogenesis due to TILT (more than $5\text{ }^{\circ}\text{C}/100\text{ km}\times 10^{-7}\text{ s}^{-1}$ on average in the ABFZ core). An elongated frontogenetic zone associated with TILT is found along the Angolan coast from 17°S to 11°S and corresponds to the upwelling tongue observed in the Angola current region (Fig.3). On the other hand, TILT is frontolytic off the ABFZ (at 17°S, 11°E) where the

downwelling is dominant as shown in Fig.3. The role of the upwelling in the ABFZ development will be analyzed in more details in the Section 6.2.

In addition to the mechanical terms, the thermodynamical component also shows some influences on the ABFZ. SFLX works frontogenetically just near the coast at 16°S and frontolytically south and north from the core of the ABFZ, although its contribution is almost negligible compared to the mechanical contribution. Annual-mean climatology of RESD is estimated from (3.4) where the left hand side $(\partial\theta_{oml}/\partial y)/\partial t$ is zero for climatology independent of time,

$$RESD = \frac{\partial u_{oml}}{\partial y} \frac{\partial \theta_{oml}}{\partial x} + \frac{\partial v_{oml}}{\partial y} \frac{\partial \theta_{oml}}{\partial y} + \frac{\partial w_b}{\partial y} \frac{\Delta \theta}{D} - \frac{\partial}{\partial y} \left(\frac{Q_s}{\rho C_p D} \right) \quad (5.1)$$

Note that all terms in Eq(5.1) is annual-mean climatology. On average in the core of the ABFZ, RESD shows a strong frontolytic contribution around the core of the ABFZ (Fig. 4e). On the other hand, frontogenesis is located in the southern part of the ABFZ. This may be due to, at least partly, vertical mixing at the base of the OML accounted for in RESD. In particular, GC2014 showed that for the SST front associated with the equatorial Atlantic cold tongue, the turbulent mixing (surface and thermocline heat fluxes) is frontolytic.

5.2 Seasonal Cycle

In the preceding subsection, we have shown that in terms of climatological annual-mean CONF and TILT of the OFGF were the main sources for the ABFZ generation. Next, we analyze the annual cycle of the ABFZ and its relationship to the seasonal variations of the OFGF terms. As shown in Fig.2, the seasonal cycle of the

ABFZ exhibits two peaks. Note that if the seasonal cycle is sinusoidal, Eq. 3.4 implies $\pi/2$ out of phase between the OFGF and temperature meridional gradient. This means that for a semi-annual oscillation the temperature meridional gradient should shift the OFGF by approximately 1 and half months.

Figure 5a illustrates the box-mean (10 °E-12 °E and 17 °S-15 °S) time series of the meridional gradient of temperature obtained from satellite and reanalysis products (the time series is smoothed by a 11-days-mean moving filter). This box covers the maximum of the ABFZ in each month since the meridional location of the ABFZ is almost stable in climatological seasonal cycle. There is an obvious semi-annual cycle of the ABFZ with maxima in April-May and in November-December, and minima in February-March and July-August, respectively (see also Fig.2). The first maximum develops rapidly (during 2 month, from March to April) whereas the development of the second maximum is somewhat slower (3 months, from August to October). Figure 5a also evidences that CFSR reproduces realistically the semi-annual cycle, although the magnitudes of the CFSR meridional SST gradient are generally slightly stronger with respect to OISST. Corresponding to the annual cycle of the ABFZ, there is a seasonal cycle of frontogenesis and frontolysis in Fig. 5a as the tendency of the ABFZ (green line): two maxima in frontogenesis in March-April and September-October and in frontolysis in May-June and December-February. The tendency of the ABFZ is estimated by Equation of 5.2.

We further analyze the seasonal cycle of the OFGF terms. Similarly to the climatological state in Fig. 4, the contributions of SHER and SFLX are relatively small and do not seem to be responsible for either of the two peaks in the ABFZ annual cycle (not shown). Figure 5b shows the seasonal variations of TILT, CONF, and RESD averaged over the same box as the temperature gradients in Fig. 5a. For

estimation of seasonal variation of RESD, the tendency of the meridional gradient is calculated as,

$$\frac{\partial}{\partial t} \left(\frac{\partial \theta_{oml}(t)}{\partial y} \right) = \frac{\frac{\partial \theta_{oml}(t+\Delta t)}{\partial y} - \frac{\partial \theta_{oml}(t-\Delta t)}{\partial y}}{2\Delta t}, \quad (5.2)$$

where, t and Δt denotes each time step and difference in time step, in this case, Δt is one day (86400 seconds). With this tendency at each day, $RESD(t)$ is estimated by

$$RESD(t) = \frac{\partial}{\partial t} \left(\frac{\partial \theta_{oml}(t)}{\partial y} \right) - SHER(t) - CONF(t) - TILT(t) - SFLX(t).$$

From the middle of November to February, the box-averaged CONF is modestly negative, which is due to the frontolytic effect adjacent to the Angolan coast as shown in Fig. 4b (however, CONF is frontogenetic off the ABFZ). The contribution of CONF becomes positive from March, although its frontogenetic contribution is relatively weak ($< 1.0 \text{ }^{\circ}\text{C}/100 \text{ km} \times 10^{-7} \text{ s}^{-1}$) until July. From the end of July CONF starts to increase and reaches its maximum ($3.0 \text{ }^{\circ}\text{C}/100 \text{ km} \times 10^{-7} \text{ s}^{-1}$) in the end of August. The frontogenetic contribution of CONF remains strong until the beginning of October but then rapidly decrease to become frontolytic in November.

The contribution of TILT to the ABFZ seasonal cycle is almost always frontogenetic. Close to zero in January, TILT is enhanced from February and reaches its maximum value ($3.0 \text{ }^{\circ}\text{C}/100 \text{ km} \times 10^{-7} \text{ s}^{-1}$) in March-April. In May-June, the frontogenetic effect of TILT gradually decreases (down to $1.0 \text{ }^{\circ}\text{C}/100 \text{ km} \times 10^{-7} \text{ s}^{-1}$) until December. The maxima in TILT and CONF correspond to the two periods of development of the ABFZ at seasonal scale: from March to April and from August to October, respectively (Fig. 5a). This suggests that the two peaks of the ABFZ are

associated with two different mechanical terms and thus are due to two different physical processes. On the other hand, the two periods of decay of the ABFZ are consistent with the periods of weak frontogenetic and/or frontolytic contributions of both TILT and CONF (as observed by Mohrholz et al., 1999), in December-February and June-July, respectively.

In addition, RESD is almost always frontolytic with a relatively large oscillation (0.0 to -5.0 $^{\circ}\text{C}/100$ $\text{km} \times 10^{-7} \text{ s}^{-1}$) as shown in Fig.5b. In particular, the frontolytic effect due to RESD is stably strong (around -3.0 $^{\circ}\text{C}/100$ $\text{km} \times 10^{-7} \text{ s}^{-1}$) from May to August when the ABFZ becomes weakened and frontogenetic effects due to CONF and TILT are relatively weak (Figs. 5a and b). Conversely as TILT and CONF, RESD does not exhibit a clear signal of semi-annual cycle, but rather an annual-cycle. We thus can conclude that in terms of a first-order estimation, the semi-annual cycle of the ABFZ is explained by the combination of TILT and CONF.

6. Discussion

The previous section showed that the two periods of development of the ABFZ in March-April and August-October were due to a large extent to the contribution of TILT and CONF, respectively. In this section, we investigate what components are responsible for the corresponding peaks in TILT and CONF.

6.1 Meridional Confluence

CONF represents changes in the meridional temperature gradient associated with ocean dynamics of convergence/divergence of meridional current, $\partial v_{oml} / \partial y$.

342 Figure 6a presents the annual cycle of $\partial v_{oml} / \partial y$ averaged over the ABFZ. In the
 343 ABFZ, the meridional current is almost always convergent except for weak
 344 divergence from November to January. The convergence of the meridional current is
 345 maximum from August to mid-October (up to $-3.0 \times 10^{-7} \text{ s}^{-1}$) and is rapidly weakened
 346 during November. The seasonal fluctuations in the convergence are associated with
 347 changes in intensity and meridional extension of the southward Angola Current and
 348 northward Benguela Current that meet in the ABFZ. Around the ABFZ, an area of
 349 lower sea surface height (SSH) is formed, associated with Angola Dome (the cold
 350 dome identified by Mazeika, 1967), which shows a pronounced seasonal cycle (e.g.,
 351 Doi et al., 2007). Such well-organized SSH spatial variability induces the geostrophic
 352 current, which can contribute to the current system around the ABFZ. Therefore, here,
 353 we also focus on the SSH and corresponding geostrophic current. Figure 6b illustrates
 354 the annual cycle of OML-mean meridional current and meridional component of
 355 geostrophic current estimated from SSH at 15 °S (north of the core of the ABFZ) and
 356 17 °S (south of the core of the ABFZ) averaged between 10 °E and 12 °E. At 15 °S the
 357 OML-mean meridional current is southward all year round, except the beginning of
 358 May when a weak northward flow is observed. The maximum southward meridional
 359 velocity occurs in October (-0.12 m/s). At 17 °S the OML-mean meridional current is
 360 northward in March-June and shows a bi-annual peak of southward current in
 361 January-to-mid-February and October indicating intrusion of tropical warm water to
 362 the ABFZ (e.g., Rouault, 2012). Figure 6b clearly evidences that the region between
 363 17 °S and 15 °S is expected to be convergent. The most convergent period is in
 364 September-October when the CONF contribution to frontogenesis is the largest as
 365 shown in Fig. 5b. Another relatively strong convergent period is from April to June
 366 when the meridional current is rather northward at 17 °S and close to zero at 15° S.

The period of weak convergence/divergence, from December to February, corresponds to frontolytic contribution of CONF (Figs.5b). Figure 6b evidences that the OML-mean meridional current can be explained, to a large extent, by the geostrophic surface current. While the large part of the meridional current and its seasonal cycle around the ABFZ is explained by geostrophic current associated with the SSH to the northwest of the ABFZ, there are some differences between v_{oml} and v_g . These differences are due to the Ekman and ageostrophic currents.

The spatial distributions of the climatological monthly mean SSH and surface geostrophic current in January, April, and September are shown in Figure 7. Two local minima of SSH are observed: one along the coast in the Benguela system and one west of the ABFZ (centered at 14 °S and 6 °E). The latter is associated with the Angola Dome (e.g., Doi et al. 2007) and a strong cyclonic geostrophic flow reaching the ABFZ. The geostrophic current generally generates the convergence in the ABFZ (Fig. 6a). However, in January an intense divergence is generated due to the strong southward ageostrophic current along the coast (Fig. 7a). In April, when CONF is modestly frontogenetic (Fig.5b), the Angola Dome and associated geostrophic flow are diminished (Fig. 7b) and a main source of convergence can thus be attributed to the northward Benguela Current which penetrates into the ABFZ as far as 16 °S. In September, whereas the low SSH sits in the south of the ABFZ as in April, the Angola Dome is significantly developed to be related to a strong geostrophic current resulting in a strong southward Angola Current intruding into the ABFZ along the Angolan coast. The northward Benguela Current is relatively weak in September compared to that in April. Thus, the maximum CONF in September is due to the strong southward Angola Current.

6.2 Tilting

TILT is the second main contributor to generate the ABFZ especially in March-to-May as shown in Figs. 4 and 5. In a first approximation TILT results from the meridional gradient of vertical motion $\partial w_b / \partial y$ convoluted with the thermocline stratification (e.g., Eq.3.4). Here, we explore more details of upwelling in the ABFZ. The annual cycle of these two components averaged over the box [12 °E-10 °E] and [17 °S-15 °S] (Fig.8) points out the **negative** $\partial w_b / \partial y$ and the **positive** stratification, respectively, from January to August. This configuration leads to frontogenesis through the TILT term (Fig. 5b). From August to December, $\partial w_b / \partial y$ changes sign and the stratification becomes weaker; that explains why the TILT term is frontolytic (especially in September) and its magnitude is weaker compared to January-August because of a weaker stratification (smaller vertical gradient in temperature). Negative $\partial w_b / \partial y$ can be seen in both March to April and August to September around the ABFZ in Figs. S1a and b, but positive $\partial w_b / \partial y$ are also generated around the ABFZ more in August-September than in March-April.

The OML depth has extrema in August to September (around 100 m) and from January to April (around 20 m) indicating the seasonal cycle of solar insolation forcing **and wind-driven mixing**. Also the intensity of the thermocline shows a strong stratification from March to May (2°C) and weak stratification from September to November (1.2°C). From March to May TILT is the most dominant frontogenetic source because the OML is the shallowest (20-30m), the stratification is the strongest (temperature jump in the thermocline up to 2.0K) and the shear of vertical velocity $\partial w_b / \partial y$ is strongly negative. The shallow OML and strong stratification can amplify the tilting effect due to $\partial w_b / \partial y$. Conversely, TILT is weakly frontolytic from August

to September when the OML-depth is deepened ($\sim 100\text{m}$), the stratification is weak (1.2K) and $\partial w_b / \partial y$ is positive. Fig.S1c and d shows the differences in OML depth and ocean stratification between March-April and August-September. Shallower OML and stronger stratification can be seen everywhere around the ABFZ. Therefore, effects of both positive and negative $\partial w_b / \partial y$ are reduced and consequently, contribution of TILT is quite weak in August to September (Fig. 5b).

7. Concluding Remarks

In this study we investigated the processes controlling the ABFZ evolution based on a first-order estimation of an ocean frontogenetic function (OFGF) applied to the ocean mixing layer (OML) derived from the CFSR reanalysis. The OFGF represents the temporal evolution of the meridional mixed-layer temperature gradient and contains three mechanical terms (shear, convergence and tilting) and one thermodynamical term. The residual term accounts for in particular vertical mixing at the bottom of the OML (which is based on parameterization of turbulence *i.e.* highly non-linear processes), entrainment velocity and horizontal/vertical advections of the meridional temperature gradient. An analysis of the annual mean OFGF suggests that the confluence effect (CONF) due to southward Angola Current (warm) and northward Benguela Current (cold) is dominantly frontogenetic over the offshore part of the ABFZ, although it has a local frontolytic effect just near the coast at 16°S . The tilting effect (TILT) related to the coastal upwelling regime is another main contributor to frontogenesis. Around the ABFZ, intense Ekman transport divergence is generated by wind stress curl (Fig. S2). This Ekman divergence induces upward motion in the Ekman layer. Interestingly, the Ekman divergence due to the zonal wind

stress is also an important contributor to the vertical velocity in the ABFZ. The contributions of the shear (SHER) and surface heat flux (SFLX) terms, are rather negligible, while the residual (RESID) term represents a main frontolytic source.

Climatological seasonal evolution of the ABFZ has a well-pronounced semi-annual cycle with two maxima of the SST meridional gradient, in April-May and November-December, and two minima, in February-March and July-August. We showed that the two maxima of the ABFZ were associated with two different mechanical terms and due to two different physical processes. The development of the first ABFZ maximum during March-April is mainly explained by the strong contribution of TILT to frontogenesis, while the development of the second ABFZ maximum during September-October is due to the frontogenetic contribution of CONF. TILT is associated with the meridional gradient of the vertical velocity. The annual maximum of TILT in March-April is due to a large extent to the combination of the maximum stratification ($\Delta\theta$), shallow OML depth (D) and negative $\partial w_b / \partial y$ during this period. Indeed, in OFGF the ratio $\frac{\Delta\theta}{D}$ represents the efficiency by which the meridional gradient of the coastal upwelling velocity can lead to the change of the ABFZ intensity. Although the OML depth also modulates the surface heat flux contribution to the OFGF, the thermodynamical term does not show any significant impact on the development of the ABFZ maximum in March-April. On the other hand, the importance of the OML depth for the thermodynamical term was suggested for frontogenesis in a SST front associated with western boundary current (Tozuka and Cronin, 2014; Tozuka et al., 2018). The annual maximum of CONF in September-October is related to an intensified southward Angola current that seems to be induced approximately by a cyclonic geostrophic flow associated with the

development of the Angola Dome (e.g., Doi et al., 2007). However, the geostrophic current is not completely consistent with the OML-mean current. The difference can be attributed to the Ekman transport and ageostrophic component. A relatively smaller contribution of CONF to frontogenesis is also observed in April and is due to the intrusion of the northward Benguela Current to the ABFZ during this period.

Most CGCMs fail to reproduce realistic SST field and ABFZ location with respect to climatology. Among other causes, this can be due to a poor representation of regional climate variables in CGCMs, such as upwelling favorable wind, wind drop off and consequently near-coastal wind curl, alongshore stratification and OML depth (e.g., Xu et al., 2014; Koseki et al., 2018; Goubanova et al., 2018), that impact directly the two main frontogenesis terms, CONF and TILT. The OFGF proposed in the present study can be thus an appropriate tool to diagnose the performance of CGCMs in the ABFZ and more generally in frontal zones. This study shows that diagnosis developed for mesoscale studies are valuable for climate studies and can help to identify the origin of biases which affect OGCMs.

Whereas the present study focused on the climatological state of the ABFZ and its seasonal cycle, the intensity and the location of the ABZF exhibits a strong inter-annual variability (e.g., Mohrholz et al., 1999; Rouault et al., 2017). The further investigation on how the contributions of the OFGF are modified in the case of Benguela Niño/Niña would provide further insight on the dynamics of the South-Eastern Tropical Atlantic and sources of the CGCMs bias which have been suggested to develop as inter-annual warm events (e.g., Xu et al., 2014).

Effects of the turbulent mixing and the effect due to the entrainment velocity at the mixed-layer base on frontogenesis were accounted by the residual of the

frontogenetic function. An accurate quantification of these effects requires using simulations of a higher resolution ocean model for which the output of the temperature tendency due to those processes are available. According to Giordani and Caniaux (2014), the vertical mixing is also large contributor to the frontogenesis. However by destroying the balance between the mass and circulation fields, the assimilation procedure induces spurious effects on the entrainment processes which justifies that this process was included in the residual term RESD. These are the main limitations of this study because diapycnal mixing is often an important term of the oceanic upper-layers heat budget which is tightly coupled with vertical motions (Giordani et al., 2013). A more comprehensive understanding of this term would be valuable to estimate the performance of CGCMs in the ABFZ and more generally in coastal upwelling zones.

Acknowledgement

We greatly appreciate two anonymous reviewers for their constructive and helpful comments. Also, we would like to express our appreciation to Dr. Kunihiro Aoki in the University of Tokyo for his constructive discussion in the beginning of stage of this study. We also thank to Dr. Guy Caniaux in Météo-France for their helpful discussions. We utilized the versions of 2012Rb of MATLAB software package provided by The MathWorks, Inc., (<http://www.mathworks.com>) and Grid Analysis and Display System (GrADS, <http://www.iges.org/grads/>) to compute each dataset and create figures. S. Koseki has received funding from the EU FP7/2007-2013 under grant agreement to no. 603521 (EU-PREFACE). K. Goubanova was also supported by Fondecyt (Grant 1171861).

512

513

514 **Reference**

515 Auel, H., and Verheye, H. M.: Hypoxia tolerance in the copepod *Calanoides*

516 *carinatus* and the effect of an intermediate oxygen minimum layer on copepod

517 vertical distribution in the northern Benguela Current upwelling system and the

518 Angola-Benguela Front. *J. Exp. Mar. Bio. Eco.*, **352**, 234-243,

519 doi:10.1026/j.jembe.2007.07.020, 2007.

520 Chavez, F. P., and Messié, M.: A comparison of eastern boundary upwelling

521 ecosystem. *Prog. Oceanogr.*, **83** (1-4), 80-96 (Dec,

522 <http://www.sciencedirect.com/science/article/pii/S0079661109000998>, 2009.

523 Chelton, D.B., and Xie, S.-P.: Coupled ocean-atmosphere interaction at ocean

524 mesoscales. *Oceanography*, **23**(4), 52-69, doi:10.5670/oceanog.2010.05, 2010

525 Chen, Z., Yan, X.-H., Jp, Y.-H., Jiang, L., and Jiang, Y.: A study of Benguela upwelling

526 system using different upwelling indices derived from remotely sensed data.

527 *Continental Shelf Research*, **45**, 27-33, 2012.

528 Colberg, F., and Reason, C. J. C.: A model study of the Angola Benguela Frontal

529 Zone: Sensitivity to atmospheric forcing. *Geophys. Res. Lett.*, **33**, L19608,

530 doi:10.1029/2006GL027463, 2006.

531 Colberg, F., and Reason, C. J. C.: A model investigation of internal variability in

532 the Angola Benguela Forntal Zone. *J. Geophys. Res.*, **112**, C07008,
533 doi:10.1029/2006JC003920, 2007.

534 Dinniman, M. S., and Rienecker, M. M.: Frontogenesis in the North Pacific Ocean
535 Frontal Zones-A Numerical Simulation. *J. Phy. Oceanogra.*, **29**, 537-559, 1999.

536 Doi, T., T. Tozuka, Sasaki, H., Masumoto, Y., and T. Yamagata, T.: Seasonal and
537 interannual variations of oceanic conditions in the Angola Dome.
538 *J. Phys. Oceanogr.*, **37**, 2698-2713, doi:10.1175/2007JPO3552.1, 2007.

539 Fennel, W., Junker, T., Schmidt, M., and Mohrholz, V.: Response of the Benguela
540 upwelling system to spatial variations in the wind stress. *Continental Shelf Research*,
541 **45**, 65-77, 2012.

542 Florenchie, P., Lutjeharms, J. E., Reason, C. J. C., Masson, S., and Rouault, M.:
543 The source of Benguela Ninos in the South Atlantic Ocean.
544 *Geophys. Res. Lett.*, **30**, doi:10.1029/2003GL017172, 2003.

545 Gammelsrød, T., Bartholomae, C. H., Boyer, D. C., Filipe, V. L. L., and O'Toole, M. J.:
546 Intrusion of warm surface water along the Angolan-Namibian coast in
547 February-March 1995: the 1995 Benguela Nino.
548 *South African Journal of Marine Science*,
549 **19:1**, 41-56, doi:10.2989/025776198784126719, 1998.

550 Giordani, H., and Caniaux, G.: Sensitivity of cyclogenesis to sea surface temperature in
551 the Northwestern Atlantic. *Mon. Wea. Rev.*, **129**(6), 1273-1295, 2001.

552 Giordani, H., and Caniaux, G.: Diagnosing vertical motion in the Equatorial Atlantic.
553 *Ocean Dynamics*, **61**(12), doi:10.1007/s10236-01—0467-7, 2012.

554 Giordani, H., Caniaux, G., and Voldoire, A.: Intraseasonal mixed-layer heat
555 budget in the equatorial Atlantic during the cold tongue development 2006.
556 *J. Geophys. Res.*, **118**, 650-671, doi:10.1029/2012JC008280, 2013.

557 Giordani, H., and Caniaux, G.: Lagrangian sources of frontogenesis in the equatorial
558 Atlantic front, *Clim. Dyn.*, doi:10.1007/s00382-014-2293-3, 2014.

559 Goubanova, K., Illig, S., Machu, E., Garcon, V., and Dewitte, B.: SST subseasonal
560 variability in the central Benguela upwelling system as inferred from satellite
561 observation (1999-2009). *J. Geophys. Res.*, **118**, 4092-4110,
562 doi:10.1002/jgrc.20287, 2013.

563 Goubanova, K., Sanchez.Gomez, E., Frauen, C., and Voldoire A.: Role of remote and
564 local wind stress forcing in the development of the warm SST errors in the
565 southeastern tropical Atlantic in a coupled high-resolution seasonal hindcast,
566 *Clim. Dyn.*, doi:10.1007/s00382-018-197-0, 2018.

567 Griffies, S. M., Harrison, M. J., Pacanowski, R. C., and Rosati, A.: Technical guide
568 to MOM4. GFDL Ocean Group Technical Report No.5, 337 pp. [Available online at
569 www.gfdl.noaa.gov/-fms], 2004.

570 Hansingo, K., and Reason, C. J. C.: Modelling the atmospheric response over southern

571 Africa to SST forcing in the southeast tropical Atlantic and southwest subtropical
572 Indian Oceans. *Int. J. Climatol.*, **29**, 1001-1012, doi:10.1002/joc.1919, 2009.

573 Hastenrath, S. and Lamb, P.: On the dynamics and climatology of surface flow over the
574 equatorial oceans. *Tellus*, **30**, 436-448, 1978.

575 Hirst, A. C., and Hastenrath, S.: Atmosphere-Ocean Mechanisms of Climate
576 Anomalies in the Angola-Tropical Atlantic Sector. *J. Phys. Oceanogr.*, **13**,
577 1146-1157, doi:http://dx.doi.org/10.1175/1520-
578 0485(1983)013<1146:AOMOCA>2.0.CO;2, 1983.

579 Junker, T., M. Schmidt, and Mohrholz, V.: The relation of wind stress curl and
580 meridional transport in the Benguela upwelling system. *J. Marine. Res.*, **143**, 1-6,
581 2015

582 Junker, T., Mohrholz, V., Siegfried, L., and van der Plas, A.: Seasonal to interannual
583 variability of water mass characteristics and current on the Namibian shelf.
584 *J. Mar. Syst.*, **165**, 36-46, doi:10.1016/j.jmarsys.2016.09.003, 2017.

585 Kay, E., Eggert, A., Flohr, A., Lahajnar N., Nausch, G., Nuemann, A., Rixen, T., Schmidt, M.,
586 Van der Pla, A., and Wasmund, N., 2018. Biogeochemical processes and turnover
587 rates in the Northern Benguela Upwelling System. *J. Mar. Syst.*, **188**, 63-80.

588 Kazmin, A. S., and Rienecker, M. M.: Variability and frontogenesis in the large-scale
589 oceanic frontal zones. *J. Geophys. Res.*, **101**, 907-921, 1996.

590 Keyser, D., Reeder, M. J., and Reed, R. J.: A Generalization of Petterssens's

591 Frontogenesis Function and Its Relation to the Forcing of Vertical Motion.
592 *Mon. Wea. Rev.*, 116, 762-780, 1988.

593 Klein S. A., and Hartmann, D. L.: The Seasonal Cycle of Low Stratiform Clouds.
594 *J. Climate*, **6**, 1587-1606, 1993.

595 Koseki, S., Keenlyside, N., Demissie, T., Toniazzo, T., Counillon, F., Bethke, I., Ilicak, M.,
596 and Shen, M.-L.: Causes of the large warm SST bias in the Angola-Benguela Frontal
597 Zone in the Norwegian Earth System Model. *Clim. Dyn.*, **50**, 4651-4670,
598 doi:10.1007/s00382-017-3896-2, 2018.

599 Kopte, R, Brandt, P., Dengler, M., Tchupalanga, P. C. M., Macueria, M., and Ostrowski, M.
600 : The Angola Current: Flow and hydrographic characteristic as observed at 11°S.
601 *J. Geophys. Res. Oceans*, **122**, 1177-1189, doi:10.1002/2016JC012374, 2017.

602 Lutz, K., Jacobeit, J., and Rathmann, J.: Atlantic warm and cold water events and
603 impact on African west coast precipitation. *Int. J. Climatol.*, **35**, 128-141,
604 doi:10.1002/joc.3969, 2015.

605 Manhique, A.J., Reason, C. J. C., Silinto, B., Zucula, J., Raiva, I., Congolo, F., and
606 Mavume, A. F.: Extreme rainfall and floods in southern Africa in January 2013 and
607 associated circulation patterns. *Nat. Hazards*, **77**, 679-691, doi:10.1007/s11069-015-
608 1616-y, 2015.

609 Mazeika, P. A., 1967: Thermal domes in the eastern tropical Atlantic Ocean. *Limnol.*
610 *Oceanogr.*, **12**, 537-539.

611 Mohrholz, V., Schmidt, M., Lutjeharms, J. R. E., and John, H.-C.H.: Space-time
 612 behavior of the Angola-Benguela Frontal Zone during the Benguela Nino of
 613 April 1999. *Int. J. Remote Sensing*, **25**, 1337-1400,
 614 doi:10.1080/01431160310001592265, 2004.

615 Patricola, C. M., and Chang, P.: Structure and dynamics of the Benguela low-level coast
 616 jet. *Clim. Dyn.*, doi:10.1007/s00382-016-3479-7, 2016.

617 Pfeifroth, U., Hollmann, R., and Ahrens, B.: Cloud Cover Diurnal Cycles in Satellite
 618 Data and Regional Climate Model Simulations.
 619 *Meteorologische Zeitschrift*, **21**, 551-560, 2012.

620 Risien, C. M., and Chelton, D. B.: A global climatology of surface wind and wind stress
 621 fields from 8 years of QuikSCAT scatterometer data. *J. Phy. Oceano.*, **38**, 2379-2413,
 622 2008.

623 Rouault, M., Florenchie, P., Fauchereau, N., and Reason, C. J. C.: South east
 624 tropical Atlantic warm events and southern African rainfall.
 625 *Geophys. Res. Lett.*, **30**, 8009, doi:10.1029./2002GL014840, 2003.

626 Rouault, M.: Bi-annual intrusion of tropical water in the northern Benguela upwelling.
 627 *Geo. Phys. Lett.*, **39**, L12606, doi:10.1029/2012GL052099, 2012.

628 Rouault, M., Illig, S., Lübbecke, J., and Koungue, R. A. I.: Origin, development and
 629 demise of the 2010-2011 Benguela Niño. *J Mar. Syst.*,
 630 <http://dx.doi.org/10.1016/j.jmarsys.2017.07.007>, 2017.

631 Saha S., and Co-authors.: The NCEP Climate Forecast System Reanalysis.
632 *Bull. Ame. Meteor. Soc.*, doi:10.1175/2010BAMS3001.1, 2010.

633 Santos, F., Gomez-Gesteria, M., deCastro, M., and Alvarez, I.: Differences in coastal and
634 oceanic SST trends due to the strengthening of coastal upwelling along the Benguela
635 current system. *Continental Shelf Research*, **34**, 79-86, 2012.

636 Small, R. J., Thomas, R. A., and Bryan, F. O.: Storm track response to Ocean Fronts in a
637 global high-resolution climate model. *Clim. Dyn.*, doi:10.1007/s00382-013-1980-9,
638 2014.

639 Stommel, H.: The Gulf Stream: a physical and dynamical description. 2nd ed. University
640 of California Press, Berkley and Cambridge University Press, London, 1965.

641 Tozuka, T., and Cronin, M. G.: Role of mixed layer depth in surface frontogenesis: The
642 Agulhas Return Current front. *Geophys. Res. Lett.*, doi:10.1002/2014GL059624,
643 2014

644 Tozuka, T., Ohishi, S., and Cronin, M. G.: A metric for surface heat flux effect on
645 horizontal sea surface temperature gradients. *Clim. Dyn.*, **51**, 547-561,
646 doi:10.1007/s00382-017-3940-2, 2018.

647 Veitch, J. A., Florenchie, P., and Shillington, F. A.: Seasonal and interannual
648 fluctuations of the Angola-Benguela Frontal Zone (ABFZ) using 4.5 km
649 resolution satellite imagery from 1982 to 1999. *Int. J. Remote Sensing*, **27**,
650 987-998, doi:10.1080/01431160500127914, 2006.

Vizy, E. K., Cook, K. H., and Sun, X.: Decadal change of the south Atlantic ocean
 Angola-Benguela forntal zone since 1980. *Clim. Dyn.*,
<https://doi.org/10.1007/s00382-018-4077-7>, 2018.

Xu Z., Chang, P., Richter, I., Kim, W., and Tang, G.: Diagnosing southeast tropical
 Atlantic SST and ocean circulation biases in the CMIP5 ensemble. *Clim. Dyn.*, **43**,
 3123-3145, doi:10.1007/s00382-014-2247-9, 2014.

Figures

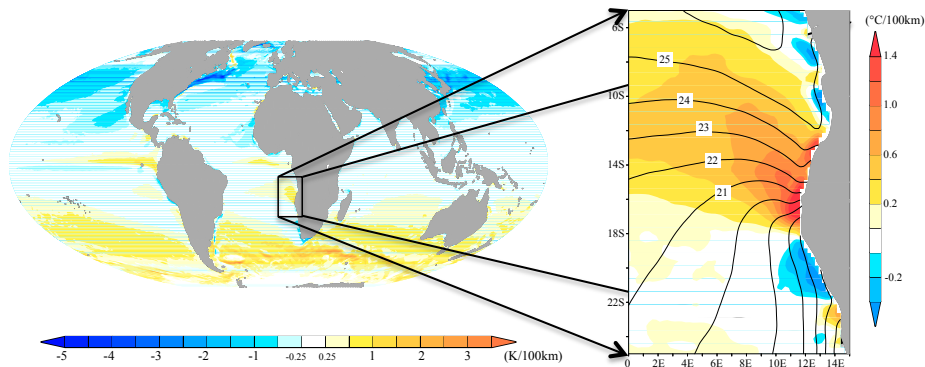


Figure 1.
 (Left) Global image of observed annual-mean SST meridional gradient from 1982-2010 of OISST. (Right) annual-mean SST
 (contour, °C) and its meridional gradient (°C/100km) around the ABFZ.

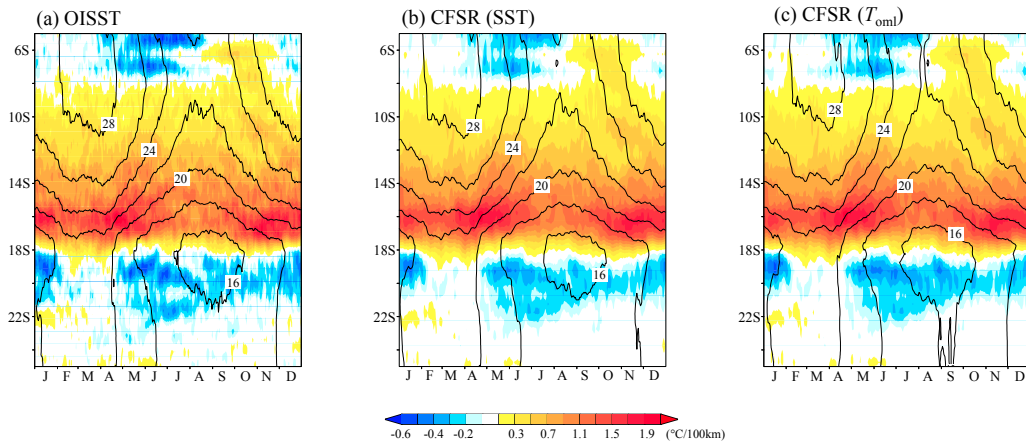


Figure 2. Climatological seasonal cycle of the temperature (contour) and its meridional gradient averaged between 10°E and 12°E for (a) SST of OISST, (b) SST of CFSR, and (c) OML-mean potential temperature of CFSR.

661

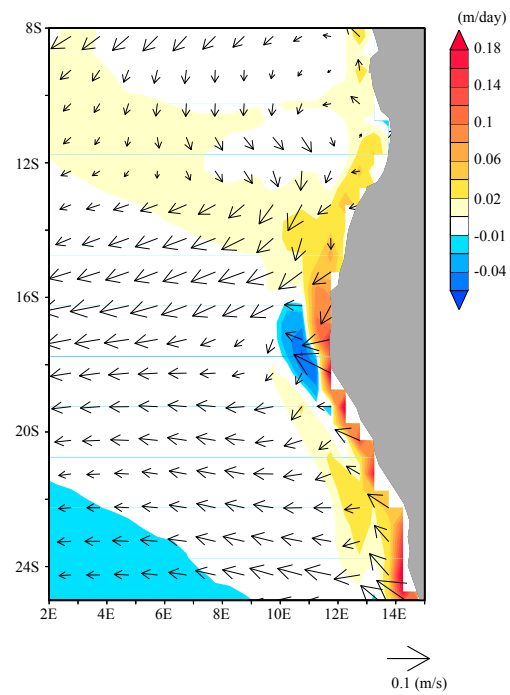


Figure 3. Annual-mean climatological states of OML-mean horizontal current (arrows) and vertical velocity at the bottom of OML (color).

662

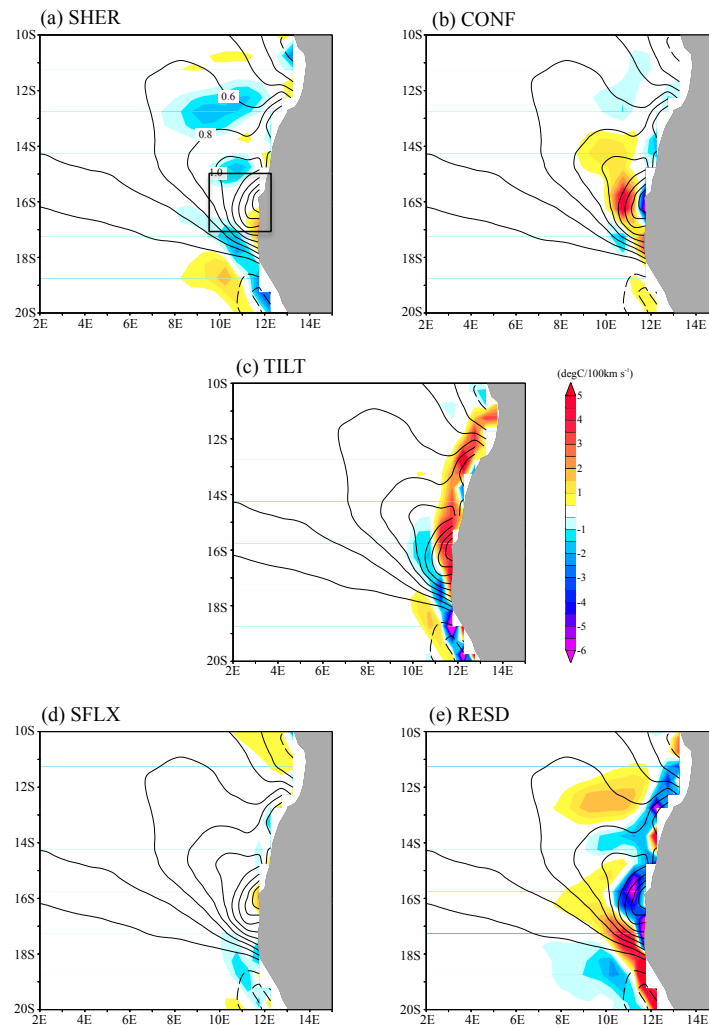


Figure 4. Annual-mean climatology of each term in OFGF. Contour is annual-mean climatology of meridional gradient of OML-mean potential temperature of CFSR (°C/100km). The black box on (a) is the ABFZ used for the analysis in this study.

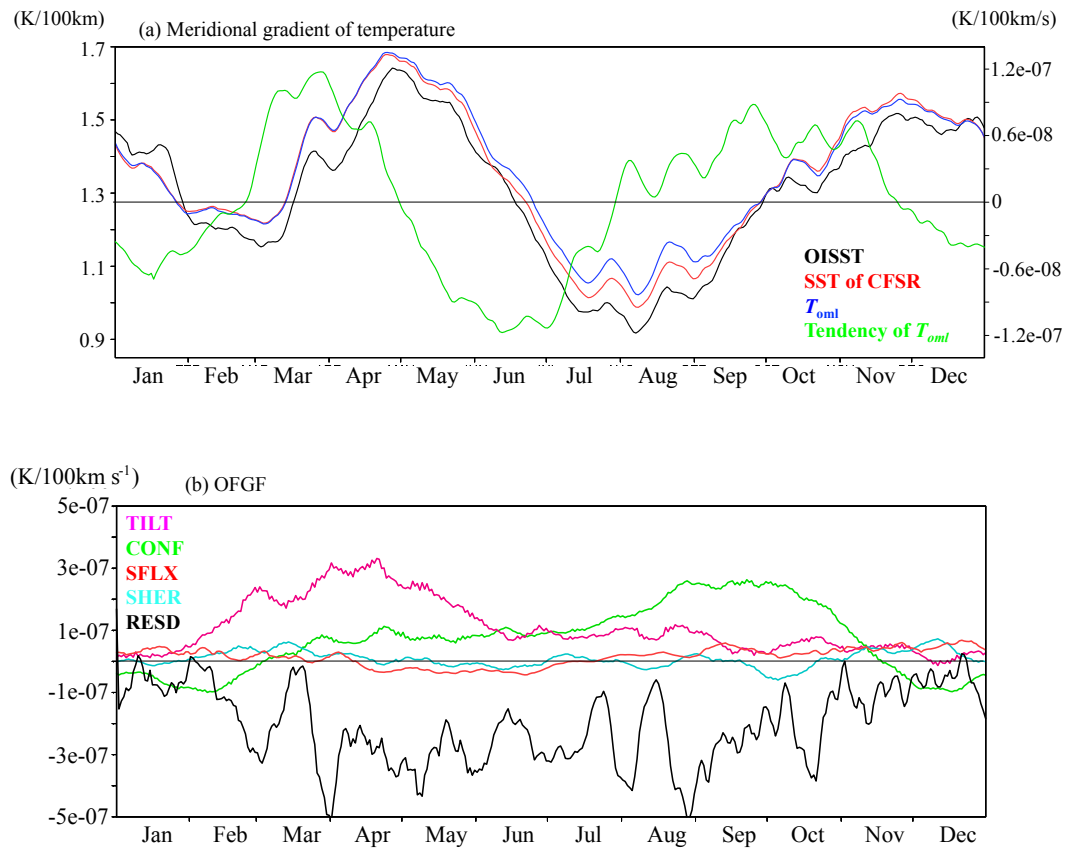


Figure 5. Box-mean (17°S-15°S and 10°E-12°E) time series of (a) meridional gradient of temperature (black: OISST, red: SST of CFSR, and blue: OML-temperature of CFSR) and (b) TILT (magenta), CONF (green), SHER (cyan), SFLX (red), and RESD (black). 11days-running mean are shown for all the time series.

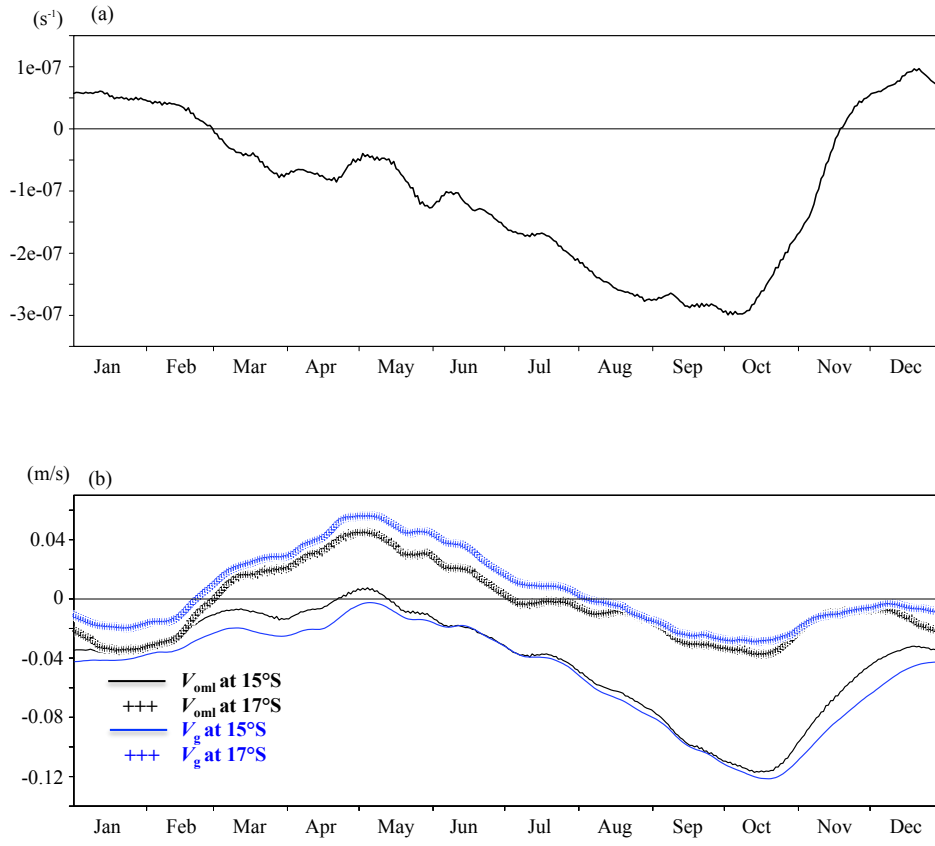


Figure 6. Time series of (a) $\partial v_{oml} / \partial y$ averaged over (17°S-15°S and 10°E-12°E) and (b) OML-mean meridional current velocity (black) and geostrophic meridional current velocity estimated from sea surface height (blue) at 15°S (solid line) and 17°S (+ mark) averaged between 10°E and 12°E. All variables are filtered by moving 11-days window.

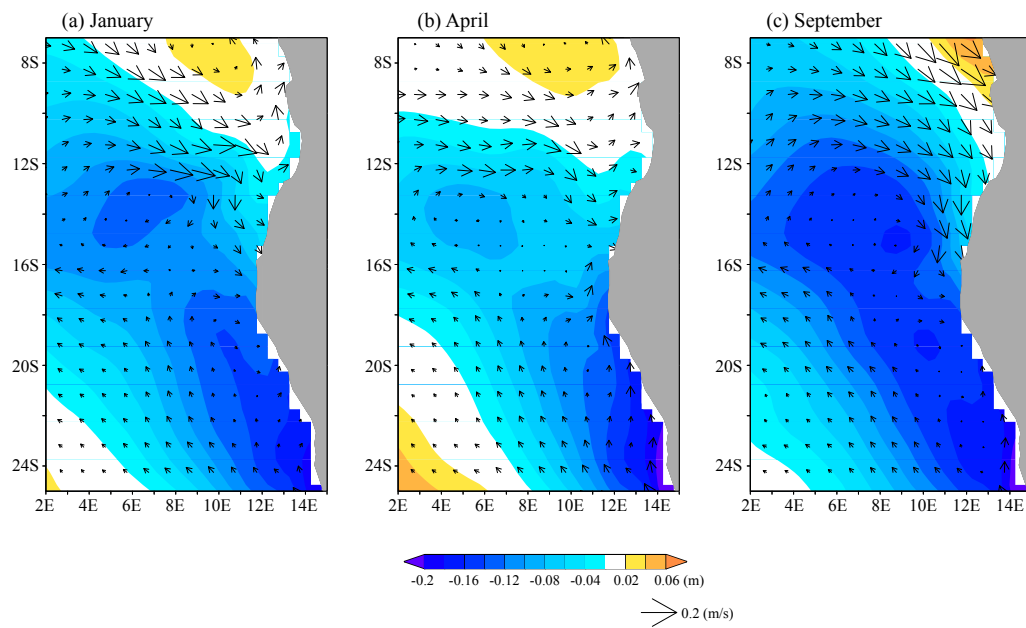


Figure 7. Monthly mean SSH (color) and geostrophic current (arrows) for (a) January, (b) April, and (c) September.

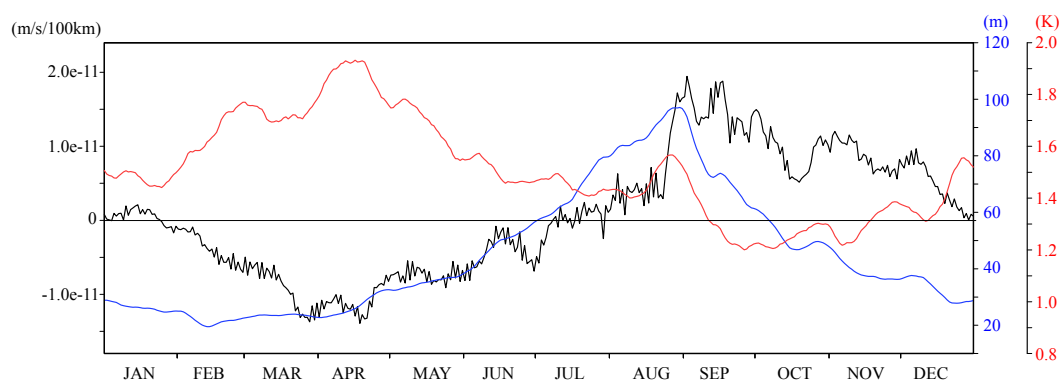


Figure 8. Time series of the area-averaged meridional gradient of the vertical velocity at the bottom of OML (black), OML depth (blue), intensity of upper ocean thermocline stratification (red) over 17°S-15°S and 10°E-12°E. All variables are filtered by moving 11-days window.

668

669